香港中文大學
The Chinese University of Hong Kong

MAEG5160: Design for Additive Manufacturing

Lecture 11: Extensions and Applications – continue - 2

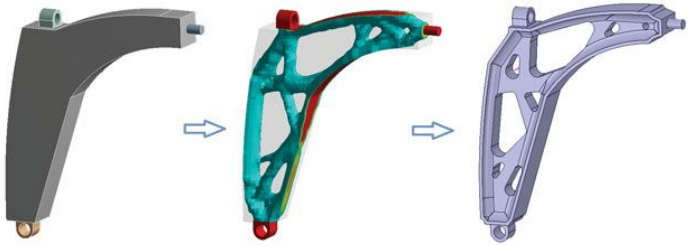

Prof SONG Xu

Department of Mechanical and Automation Engineering,
The Chinese University of Hong Kong.

Lecture 11: Extensions and Applications – continue - 2

8. Alternative physics problems

The computational procedures for topology optimization were originally developed for the design of elastic structures, but its theoretical inspiration came to a large extend from work carried out for plates and for scalar problems such as conduction problems (heat or electricity). The application of numerical methods for topology optimization for these problems is with today's knowledge rather straightforward, and the computations are typically less time consuming due to the simpler FE analysis models. We note here that all the theoretical considerations required for the elasticity case (mesh dependence, the role of composites, etc.) have parallels for the scalar situation; actually much more theoretical insight has been gained for this setting. In recent years, topology design methods have also been expanded to for example electro-magnetic problems, coupled problems, fluid problems, and wave propagation problems. Here and in later sections of this chapter we illustrate some of these settings.

Lecture 11: Extensions and Applications – continue - 2

8.1 Multiphysics problems

The phrase "multiphysics problems" covers optimization problems that require modelling in several areas of physics. Apart from making the modelling more complicated due to coupling effects, it also complicates the sensitivity analysis. However, with the help of the adjoint method, it is always possible to perform the sensitivity analysis in an efficient way as long as the objective function is a global description of the response.

We will demonstrate the sensitivity analysis for multiphysics problems on a simple weakly coupled linear problem involving two fields (for example heat conduction and elasticity). The FE-equations of the two systems are given by

$$\mathbf{K}_1\mathbf{u}_1 = \mathbf{f}_1 \qquad \text{and} \qquad \mathbf{K}_2\mathbf{u}_2 = \mathbf{f}_2(\mathbf{u}_1)$$

where it is assumed that system 2 (the elastic problem) is weakly dependent on system 1 (the thermal field) and that both system matrices depend on the design variables. This means that we have to solve system 1 and insert the solution in the load vector of system 2. Physically, it means that the temperature field gives rise to a thermal expansion that influences the elastic field . The aim is to find the sensitivity of a component of the second response vector (a displacement at a point) which can (as done previously) be written as

$$u_{out} = \mathbf{l}^T\mathbf{u}_2$$

Lecture 11: Extensions and Applications – continue - 2

Using the adjoint method, we proceed as follows. We start by adding two null terms to the original expression

$$u_{out} = \mathbf{l}^T \mathbf{u}_2 + \boldsymbol{\lambda}_1 \left[\mathbf{K}_1 \mathbf{u}_1 - \mathbf{f}_1\right] + \boldsymbol{\lambda}_2 \left[\mathbf{K}_2 \mathbf{u}_2 - \mathbf{f}_2(\mathbf{u}_1)\right] \ ,$$

where λ_1 and λ_2 are arbitrary, fixed vectors. The sensitivity of this augmented expression is

$$\frac{\partial u_{out}}{\partial \rho_e} = \mathbf{l}^T \frac{\partial \mathbf{u}_2}{\partial \rho_e} + \boldsymbol{\lambda}_1^T \left(\frac{\partial \mathbf{K}_1}{\partial \rho_e}\mathbf{u}_1 - \frac{\partial \mathbf{f}_1}{\partial \rho_e}\right) + \boldsymbol{\lambda}_2^T \left(\frac{\partial \mathbf{K}_2}{\partial \rho_e}\mathbf{u}_2 - \frac{\partial \mathbf{f}_2}{\partial \rho_e}\right) + \boldsymbol{\lambda}_1^T \mathbf{K}_1 \frac{\partial \mathbf{u}_1}{\partial \rho_e} + \boldsymbol{\lambda}_2^T \mathbf{K}_2 \frac{\partial \mathbf{u}_2}{\partial \rho_e} - \boldsymbol{\lambda}_2^T \frac{\partial \mathbf{f}_2}{\partial \mathbf{u}_1} \frac{\partial \mathbf{u}_1}{\partial \rho_e} \ .$$

To remove the field sensitivity terms $\frac{\partial \mathbf{u}_i}{\partial \rho_e}$, the following expressions should be zero

$$\left[\mathbf{l}^T + \boldsymbol{\lambda}_2^T \mathbf{K}_2\right] \frac{\partial \mathbf{u}_2}{\partial \rho_e} = 0 \quad \text{and} \quad \left[-\boldsymbol{\lambda}_2^T \frac{\partial \mathbf{f}_2}{\partial \mathbf{u}_1} + \boldsymbol{\lambda}_1^T \mathbf{K}_1\right] \frac{\partial \mathbf{u}_1}{\partial \rho_e} = 0 \ .$$

This can be achieved by selecting the adjoint vectors $\boldsymbol{\lambda}_i$ as the solution to the two adjoint problems

$$\mathbf{K}_2 \boldsymbol{\lambda}_2 = -\mathbf{l} \quad \text{and} \quad \mathbf{K}_1 \boldsymbol{\lambda}_1 = \boldsymbol{\lambda}_2^T \frac{\partial \mathbf{f}_2}{\partial \mathbf{u}_1} \ .$$

With solutions to these equations, the sensitivity expression becomes

$$\frac{\partial u_{out}}{\partial \rho_e} = \boldsymbol{\lambda}_1^T \left(\frac{\partial \mathbf{K}_1}{\partial \rho_e}\mathbf{u}_1 - \frac{\partial \mathbf{f}_1}{\partial \rho_e}\right) + \boldsymbol{\lambda}_2^T \left(\frac{\partial \mathbf{K}_2}{\partial \rho_e}\mathbf{u}_2 - \frac{\partial \mathbf{f}_2}{\partial \rho_e}\right) \ .$$

Lecture 11: Extensions and Applications – continue - 2

It is now seen that the complete analysis and associated sensitivity calculation requires that one first solves system 1, then system 2, and then for the sensitivity analysis one solves system 2 with a new (unit) load case and finally system 1 is solved with a modified load that depends on λ_1. This scheme immediately applies also to systems that involve three weakly coupled fields.

8.2 Micro-Electro-Mechanical Systems (MEMS)

In the previous introduction, we discussed the advantages of compliant mechanism in connection with MEMS applications. Modelling of MEMS typically involves simulations in multiple physical domains, for example coupled electrostatics and elasticity or coupled electric, thermal and elastic fields. The latter is required for the analysis and design of an electrothermal micro actuator. Electrothermal actuation is based on Joule's (resistive) heating and thereby thermal expansion and therefore requires modelling of three physical fields, namely electric, thermal and elastic fields. Electrothermal actuation is attractive for micro-systems due to its large displacement and force potential but the drawbacks are that it requires a strong electric field and that the operating temperature may disturb its environment.

Lecture 11: Extensions and Applications – continue - 2

A typical MEMS synthesis problem is to come up with a two-degree-of-freedom device with zero cross-axis sensitivity for scanning purposes. A design problem for such an application is sketched below. The synthesis problem here consists in finding a scanning mechanism where the scanning head (output point) moves in the horizontal direction for one electric input and in the vertical direction for another electrical input. The optimization problem involves 16 "load cases", 8 constraints and 8000 design variables. The iteration history is shown in (b), the two modes of actuation are shown in (c), and an actuator built in Nickel (size *500μm* by *400μm)* which was fabricated and tested is shown in (d).

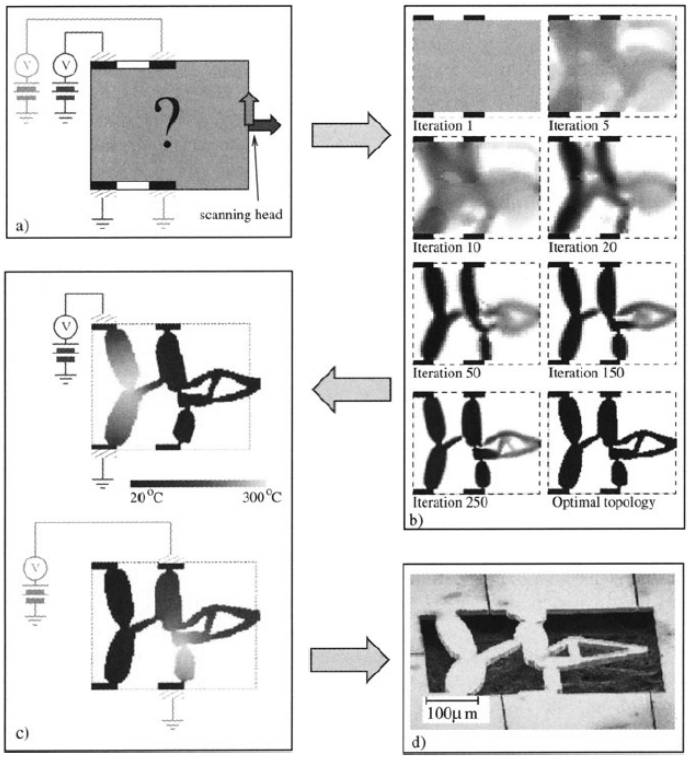

Two degree-of-freedom electro thermo mechanical actuator synthesis. a) design problem with two electrical inputs, b) iteration history, c) actuation modes and d) micro-fabricated actuator

Lecture 11: Extensions and Applications – continue - 2

8.3 Stokes flow problems

A new and very interesting application of the topology optimization method is optimization for Stokes flow problems. The finite element equations for general Stokes flow in three dimensions can be written as:

$$\begin{bmatrix} \mathbf{K} & -\mathbf{G}_F \\ -\mathbf{G}_F^T & \mathbf{0} \end{bmatrix} \begin{Bmatrix} \mathbf{u} \\ \mathbf{p} \end{Bmatrix} = \begin{Bmatrix} \mathbf{f} \\ \mathbf{0} \end{Bmatrix}, \qquad \begin{aligned} \mu\nabla^2\mathbf{u} - \boldsymbol{\nabla} p + \mathbf{f} &= \mathbf{0} \\ \boldsymbol{\nabla}\cdot\mathbf{u} &= 0 \end{aligned}$$

where $\mathbf{u}$ is the velocity vector, $\mathbf{p}$ the pressure vector, and

$$\mathbf{K} = \int_V \mu \mathbf{B}^T \mathbf{I}_0 \mathbf{B} dV, \quad \mathbf{G}_F = \int_V (\nabla \mathbf{N}_\mathbf{u})^T \mathbf{N}_p dV, \quad \mathbf{f} = \int_{\Gamma_t} \mathbf{N}_\mathbf{u}^T \, \bar{t} \, d\Gamma$$

and μ is the dynamic viscosity. $\mathbf{N}_\mathbf{u}$ and $\mathbf{N}_p$ are the usual finite element shape matrices for the velocity and pressure fields, respectively, and $\mathbf{I}_0$ is a diagonal (6 by 6) matrix with 2's on the first three diagonal entries and 1's on the last three diagonal entries

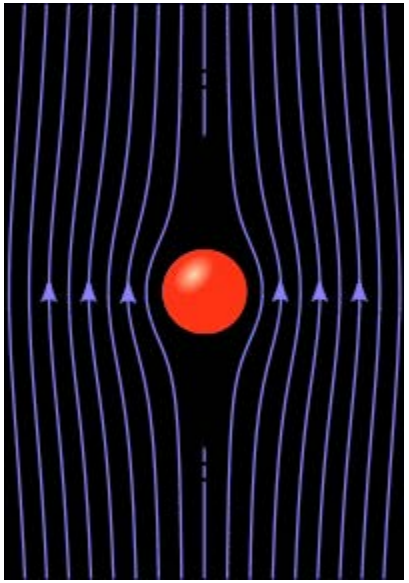

The key question is now how to optimize such kinds of problems using topology optimization. For 2D problems, it is suggested to model the flow as a Couette flow, i.e. a flow between plates with a distance of 2ρ. This means that the components of the flow vector can be written as

Lecture 11: Extensions and Applications – continue - 2

$$u_1(x_1, x_2, x_3) = \hat{u}_1(1 - \left(\frac{x_3}{\rho}\right)^2)$$
$$u_2(x_1, x_2, x_3) = \hat{u}_2(1 - \left(\frac{x_3}{\rho}\right)^2)$$
$$u_3(x_1, x_2, x_3) = 0 \ .$$

Re-deriving the finite element equations with these assumptions and dropping the hats, one gets the following matrices to insert in the general FE equation which now is 2-dimensional

$$\mathbf{K} = \int_V \mu \mathbf{B}^T \mathbf{I}_0 \mathbf{B} dV + \int_V \alpha(\rho) \mathbf{N}^T \mathbf{N} dV = \sum_e \mu \mathbf{K}_e^\mu + \sum_e \alpha(\rho) \mathbf{K}_e^\alpha \ ,$$
$$\mathbf{G}_F = \int_V (\nabla \mathbf{N}_\mathbf{u})^T \mathbf{N}_p dV \ , \qquad \mathbf{f} = \int_{\Gamma_t} \mathbf{N}_\mathbf{u}^T \ \bar{t} \ d\Gamma \ ,$$

where $\alpha(\rho) = \frac{5\mu}{2\rho^2}$.

The second term in $\mathbf{K}$ is interesting. For big ρ and therefore small α, we have an undisturbed Stokes flow. For small ρ (narrow channel) the term becomes large and may be interpreted as a large "damping" term that stops the flow. Another way to interpret the second term is to see it as a penalization term that ensures zero velocities at the penalized points – just as for the support design problem

Lecture 11: Extensions and Applications – continue - 2

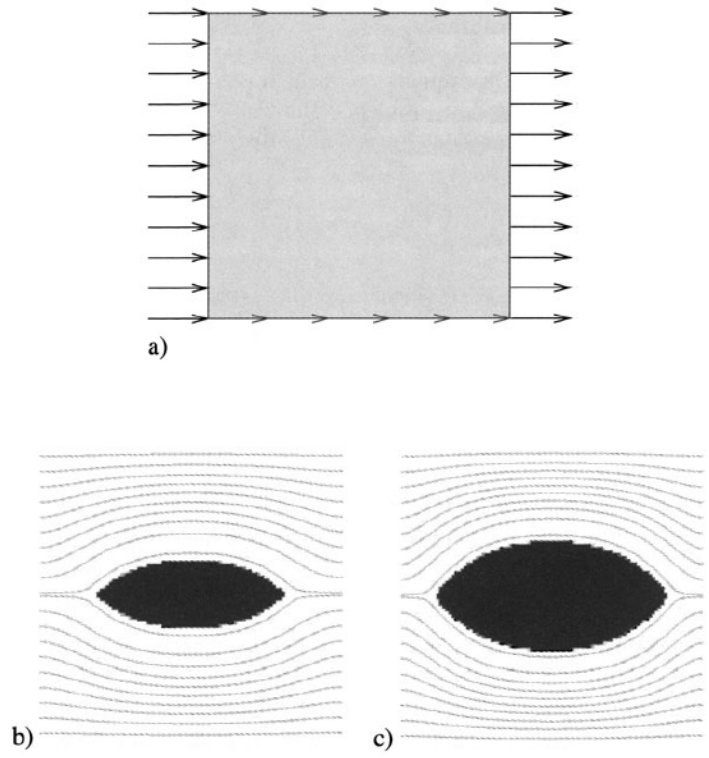

Topology optimization of Stokes flow problem. The minimum drag profiles for b) 80% and c) 90% fluid volume, respectively. The results are obtained using bi-linear 4-node elements for modelling of the velocity field and 4-node constant pressure elements for the pressure field.

Lecture 11: Extensions and Applications – continue - 2

Although this formulation was derived for two-dimensional problems, the idea generalizes to three dimensions although the physical explanation in this case is lost.

We are now ready to formulate the optimization problem. We will take $\rho_e \in]0, 1]$ as the design variable and we are allowed to use a prescribed amount of fluid in the design domain, i.e. the sum of the ρ_e's is constrained. We want to minimize the energy dissipation in the system. This corresponds to maximizing the "flow compliance" $c = \mathbf{f}^T\mathbf{u}$.

The optimization problem may now be stated as

$$\min_{\boldsymbol{\rho}} \quad -\mathbf{f}^T\mathbf{u}$$

$$\text{s.t.}: \quad \begin{bmatrix} \mathbf{K} & -\mathbf{G}_F \\ -\mathbf{G}_F^T & \mathbf{0} \end{bmatrix} \begin{Bmatrix} \mathbf{u} \\ \mathbf{p} \end{Bmatrix} = \begin{Bmatrix} \mathbf{f} \\ \mathbf{0} \end{Bmatrix} ,$$

$$\sum_{e=1}^{N} v_e\rho_e \leq V, \qquad 0 \leq \rho_e \leq 1, \quad e = 1, \ldots, N$$

The sensitivities of the objective function are simply

$$\frac{\partial c}{\partial \rho_e} = \mathbf{u}^T \frac{\partial \mathbf{K}}{\partial \rho_e}\mathbf{u} = \frac{\partial \alpha(\rho_e)}{\partial \rho_e}\mathbf{u}^T\mathbf{K}_e^{\alpha}\mathbf{u} .$$

The optimization problem is closely related to compliance minimization problems and may therefore be solved easily using an Optimality Criteria based algorithm.

Lecture 11: Extensions and Applications – continue - 2

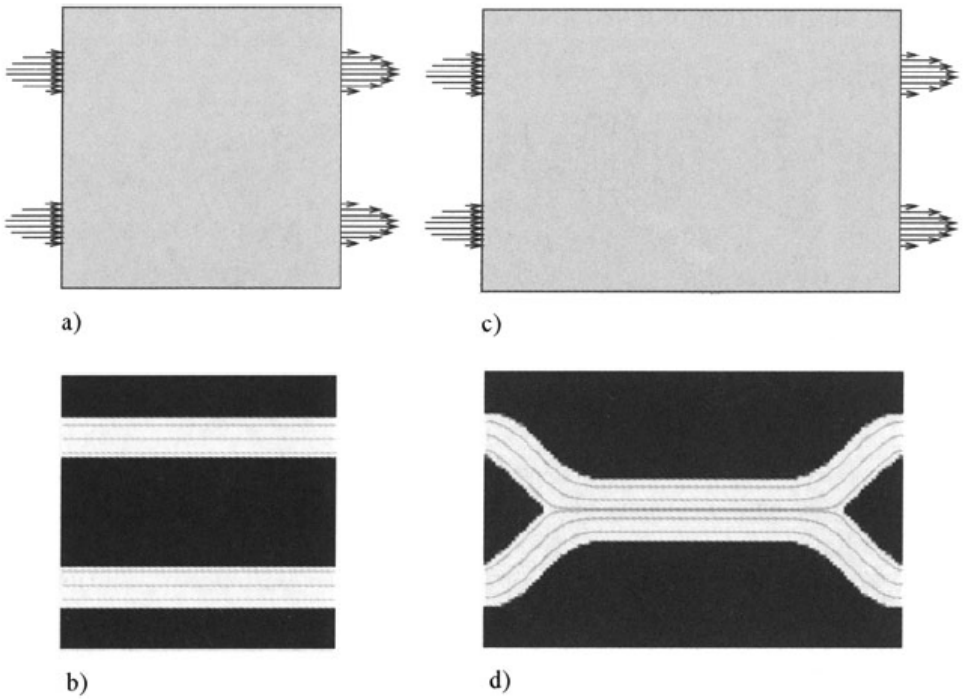

Minimization of flow resistance in a structures with two parallel inlets and outlets for 30% fluid volume. a) Design domain with aspect ratio 1:1 and solution b) . c) Design domain with aspect ratio 3:2 and solution d) . The flow resistance of d) is 22% lower than for a topology with two straight pipes as in b) due to the lower resistance of the single wide channel.

Lecture 11: Extensions and Applications – continue - 2

9. Optimal distribution of multiple material phases

Previously we discussed different ways to interpolate the stiffness of elements with intermediate densities for solid void (one material and void) compliance minimization problems. We concluded that the choice of interpolation scheme plays a role in being able to interpret intermediate variables but otherwise, many different schemes have proven equally useful in obtaining good topological solutions. When considering distribution of multiple material phases in a design domain, the choice of interpolation function becomes more critical. For stiffness interpolation there is again the risk of ending up with intermediate design elements that cannot be represented by physical materials. Worse however, there is a risk that the optimization algorithm will make use of these non-physical properties to produce artificially good structures. An example of this could be a non-physically high thermal expansion coefficient for an intermediate density element.

In the following, we first discuss alternative ways to write the stiffness interpolation for one material and void structures. Then we discuss the extensions to two material structures and finally to two material and void structures.

Lecture 11: Extensions and Applications – continue - 2

9.1 One material structures

Considering structures built from one material and void, the SIMP interpolation for stiffness can be written in either of the following ways

$$E(\rho_e) = \rho_e^p E^0 \quad \left(E_{ijkl}(\rho_e) = \rho_e^p E^0_{ijkl}\right) \ , \tag{2.29}$$

$$\left.\begin{aligned} \kappa(\rho_e) &= \rho_e^p \ \kappa^0 \ , \\ \mu(\rho_e) &= \rho_e^p \ \mu^0 \ , \end{aligned}\right\} \tag{2.30}$$

where superscript ^{0} signifies a property of the solid material, and κ and μ are the bulk and shear moduli, respectively,. Also, it is assumed in (2.29) that the Poisson's ratio is constant and equal to ν^0 . As discussed earlier the power p must be larger than a certain number dependent on

the Poisson's ratio of the material in order to satisfy the Hashin- Shtrikman bounds on elastic material behaviour

For an interpolation of scalar problems like electrical or thermal conduction we can use an interpolation as

$$\zeta(\rho_e) = \rho_e^p \zeta^0 \ ,$$

where likewise p must be bigger or equal to 2 to ensure physical realizability of intermediate density elements

Lecture 11: Extensions and Applications – continue - 2

9.2 Two material structures without void

Considering structures composed of two materials, the interpolation laws must be modified. A modification of the power-law approach is to express the elasticity tensor of element e as

$$E_{ijkl}(\rho_e) = \rho_e^p \; E^1_{ijkl} + (1-\rho_e)^p \; E^2_{ijkl} \; , \tag{2.31}$$

where E^1_{ijkl} and E^2_{ijkl} are the elasticity tensors of material 1 and 2, respectively. Although this interpolation has been used with success, it suffers a number of drawbacks. First, it violates the Hashin-Shtrikman bounds for low values of ρ_e and for large values of the power p. Furthermore, for the case of two materials with equal Young's moduli but *different* Poisson's ratios, it gives a strangely acting interpolation scheme. Finally, the scheme (2.31) changes behaviour if the phases are interchanged.

Instead of (2.31) one can use an interpolation that works with a weighted average of the Hashin-Shtrikman upper and lower bounds for each material property independently (cf., Sect. 1.5.4). The interpolated values for bulk, shear and conductivity moduli, respectively, are then written as

$$\left.\begin{aligned} \kappa(\rho_e) &= (1-\psi)\; \kappa^{HS}_{lower}(\rho_e) \; + \psi \; \kappa^{HS}_{upper}(\rho_e) \\ \mu(\rho_e) &= (1-\psi)\; \mu^{HSW}_{lower}(\rho_e) + \psi \; \mu^{HSW}_{upper}(\rho_e) \\ \zeta(\rho_e) &= (1-\psi)\; \zeta^{HS}_{lower}(\rho_e) \; + \psi \; \zeta^{HS}_{upper}(\rho_e) \end{aligned}\right\} , \tag{2.32}$$

where $(\kappa^{HS}_{lower}, \; \kappa^{HS}_{upper})$, $(\zeta^{HS}_{lower}, \; \zeta^{HS}_{upper})$ are the lower and upper Hashin-Shtrikman bounds on bulk and conductivity moduli, respectively, and $(\mu^{HSW}_{lower}, \; \mu^{HSW}_{upper})$ are the lower and upper Hashin-Shtrikman-Walpole bounds on shear modulus for two-phase composites . In (2.32), $\psi \in [0,1]$ interpolates between the lower and upper bounds. If we choose $\psi = 0$, the use of intermediate densities is made uneconomical just as in the power-law approach.

Lecture 11: Extensions and Applications – continue - 2

For design of two-phase composite involving the thermal expansion coefficient, one does not need an interpolation scheme as it is directly given in terms of the effective (interpolated) bulk modulus

$$\alpha(\rho_e) = \frac{\alpha^1\kappa^1(\kappa^2 - \kappa(\rho_e)) - \alpha^2\kappa^2(\kappa^1 - \kappa(\rho_e))}{\kappa(\rho_e)(\kappa^1 - \kappa^2)},$$

where κ^1 and κ^2 are the bulk moduli of material 1 and 2, respectively.

9.3 Two material structures with void

The two-phase power-law interpolation scheme can also be extended to a scheme for three material phases (two materials and void) with two design variables ρ_e^1 and ρ_e^2

$$E_{ijkl}(\rho_e^1, \rho_e^2) = (\rho_e^1)^{p_1}\left((\rho_e^2)^{p_2}\ E_{ijkl}^1 + (1-\rho_e^2)^{p_2}\ E_{ijkl}^2\right),$$

where the penalization powers p_1 and p_2 can be chosen independently. This modified SIMP scheme performs very well for pure stiffness problems. For use in multiphysics, however, one should apply a hybrid of the power-law and the Hashin-Shtrikman interpolation scheme, making use of the best features of both. By interpolating between material (any of the two materials) and void using the power-law approach, problems with jumps in properties are avoided and by using the Hashin-Shtrikman bounds to interpolate between the two material phases, a consistent interpolation is obtained.

Lecture 11: Extensions and Applications – continue - 2

The scheme is invoked for each property independently as

$$\left.\begin{aligned}
\kappa(\rho_e^1,\ \rho_e^2) &= (\rho_e^1)^p \left[(1-\psi)\ \kappa_{lower}^{HS}(\rho_e^2) + \psi\ \kappa_{upper}^{HS}(\rho_e^2)\right] \ , \\
\mu(\rho_e^1,\ \rho_e^2) &= (\rho_e^1)^p \left[(1-\psi)\ \mu_{lower}^{HSW}(\rho_e^2) + \psi\ \mu_{upper}^{HSW}(\rho_e^2)\right] \ , \\
\zeta(\rho_e^1,\ \rho_e^2) &= (\rho_e^1)^p \left[(1-\psi)\ \zeta_{lower}^{HS}(\rho_e^2) + \psi\ \zeta_{upper}^{HS}(\rho_e^2)\right] \ .
\end{aligned}\right\} \tag{2.34}$$

The interpolation law for the thermal expansion coefficient is just a slight modification of (2.33) and is given by

$$\alpha(\rho_e^2) = \frac{\alpha^1\ \kappa^1\ (\kappa^2 - \kappa(\rho_e^2)) - \alpha^2\ \kappa^2\ (\kappa^1 - \kappa(\rho_e^2))}{\kappa(\rho_e^2)\ (\kappa^1 - \kappa^2)}. \tag{2.35}$$

Note that the thermal expansion coefficient depends on the bulk modulus of the two-phase composite only (which is found by setting $\rho_1^e = 1$ in (2.34)).

The material interpolation scheme, defined by (2.34) and (2.35), is controlled by the two penalization parameters p and Ψ. If these parameters are selected according to the criterion

$$p \geq \max\left(\frac{\kappa^1+\mu^1}{\mu^1}, \frac{\kappa^1+\mu^1}{\kappa^1}, \frac{\kappa^2+\mu^2}{\mu^2}, \frac{\kappa^2+\mu^2}{\kappa^2}\right) \ , \qquad 0 \leq \Psi \leq 1 \ , \tag{2.36}$$

then it can be shown that the interpolated parameters always will satisfy the Hashin-Shtrikman bound. Usually we choose $p = 3$ and $\Psi = 1$, corresponding to the usual power-law penalization and the upper Hashin-Shtrikman bound for the two material composite. In the cases where the upper Hashin-Shtrikman bound interpolation results in intermediate values of the second design variable, i.e. we have a two-material composite, the value of Ψ is lowered towards zero, resulting in a non-composite (and manufacturable) topology.

Lecture 11: Extensions and Applications – continue - 2

9.4 Examples of multiphase design

An example of distribution of two material phases in an L-shaped design domain is shown below. Depending On the stiffness of the second material it will act as core material (b and c) or as a structural material (d and e) .

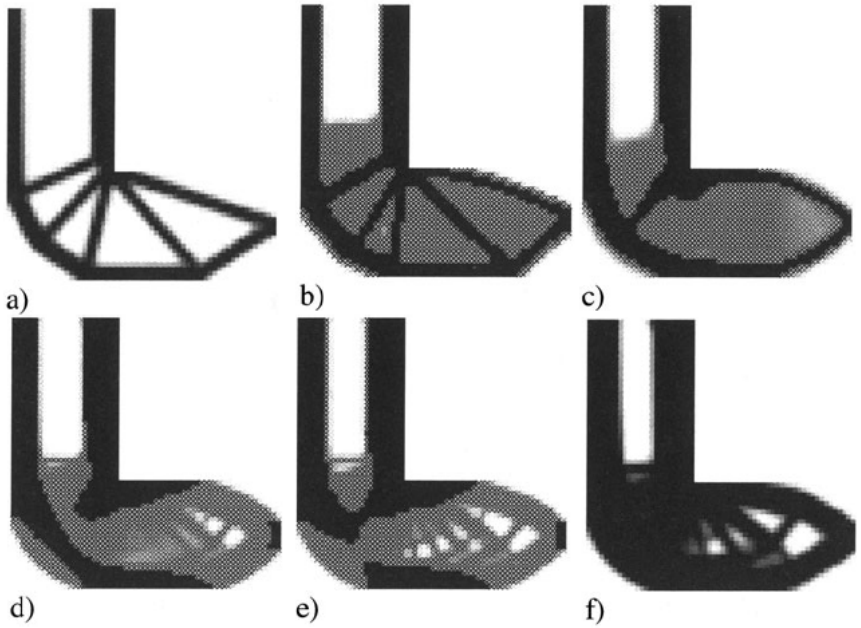

Optimal distribution of two material phases for compliance minimization of the L-shaped structure. Different ratios between the stiff (black) and the soft phase (hatched). a) Optimal distribution of 25% volume fraction of only one phase. b-e) Optimal distributions of two materials with each a volume fraction of 25%. Ratio between material stiffnesses: b) 0.01 , c) 0.2, d) 0.5 and e) 0.8. f) Optimal distribution of 50% volume fraction of only one phase.

Lecture 11: Extensions and Applications – continue - 2

10. Material design

The response of structures depends on the materials they are built from. If one can design materials with tailored or extreme properties one may be able to design better structures. This aspect is central also in topology design where the role of composites in the homogenization approach and other optimization models operating with general material tensors underlines such an aspect of *local optimal use of material*. In this section we will deal with methods that apply the ideas of topology optimization, originally developed for structural optimization problems, to the design of material design as well. The fundamental idea is that *any material is a structure if you look at it through a sufficiently strong microscope*.

Assuming that the material one considers is periodic, its effective properties may be fully described by an analysis of the smallest repetitive unit, the base cell. The design problem then consists in assigning a material type to each point in the base cell. In the discretized topology optimization setting this corresponds to assigning a material type to each element used to discretize the base cell. The material type may be selected from two or more constituent phases of which one may be void. For example, a porous honeycomb material may be designed from a void and a solid material phase.

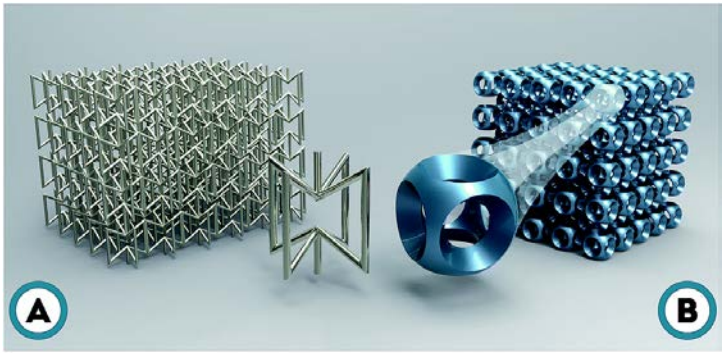

Lecture 11: Extensions and Applications – continue - 2

The effective properties of a material are found by homogenization of the microstructure. In our case the microstructure does not exist ab initio but we seek to come up with a microstructure with prescribed or extreme homogenized properties. Therefore the material design method has also been called *the inverse homogenization method*. Before we proceed to define objective functions for material design, we briefly discuss how to find the effective properties and the sensitivities thereof using the homogenization method.

10.1 Numerical homogenization and sensitivity analysis

If a structure is built from periodic materials it is often too cumbersome or even impossible to model it taking every detail of the micro-structure into consideration. Therefore, one substitutes the microstructure with some average or smeared out properties that model the material behaviour seen on a global scale. The process of finding representative or effective properties of microstructured materials is called homogenization. The homogenized stiffness tensor is by integration over the base cell area Y found as

$$E^H_{ijkl} = \frac{1}{|\mathrm{Y}|}\int_Y \left[E_{ijkl} - E_{ijpq}\frac{\partial \chi^{kl}_p}{\partial y_q}\right] \mathrm{d}y$$

where the Y-periodic test fields χ^{kl}_p are found as the solutions to the equilibrium equations

Lecture 11: Extensions and Applications – continue - 2

$$\int_{\mathrm{Y}} E_{ijpq} \frac{\partial \chi_p^{kl}}{\partial y_q} \frac{\partial \phi_i}{\partial y_j} \mathrm{d}y = \int_{\mathrm{Y}} E_{ijkl} \frac{\partial \phi_i}{\partial y_j} \mathrm{d}y \quad \text{for all Y} - \text{periodic } \phi$$

and Y is the area of the unit cell. In a somewhat simpler notation,

$$E^H_{ijkl} = \frac{1}{|\mathrm{Y}|} \int_{\mathrm{Y}} E_{pqrs} (\varepsilon^{0(ij)}_{pq} - \varepsilon^{*(ij)}_{pq})(\varepsilon^{0(kl)}_{rs} - \varepsilon^{*(kl)}_{rs}) \, \mathrm{d}y$$

where $\varepsilon^{*(kl)}_{pq} = \frac{1}{2}(\frac{\partial \chi_p^{kl}}{\partial y_q} + \frac{\partial \chi_q^{kl}}{\partial y_p})$ and ε^0_{ij} corresponds to the three (2D) or six (3D) unit test strain fields.

In practice, the equilibrium equations are solved as a finite element problem with three or six load cases

$$\mathbf{K}\boldsymbol{\chi}^{kl} = \mathbf{f}^{kl} \ ,$$

where the displacements $\boldsymbol{\chi}^{kl}$ are constrained to be Y-periodic by either a penalty approach or by assigning equal node numbers to opposing boundary nodes. The force vector is found from

$$\mathbf{f}^{kl} = \sum_e \int_{\mathrm{Y}_e} \mathbf{B}_e^T \mathbf{E}_e(\rho_e) \, \boldsymbol{\varepsilon}^{0(kl)} \mathrm{d}y \ ,$$

Lecture 11: Extensions and Applications – continue - 2

and the global stiffness matrix is calculated as the usual assembly of element stiffness matrices $\mathbf{K} = \sum_e \mathbf{K_e}$ plus corrections for periodicity. In FE-notation, the effective properties may then be found as

$$E^H_{ijkl} = \frac{1}{|\mathrm{Y}|} \sum_e (\boldsymbol{\chi}^{0(ij)} - \boldsymbol{\chi}^{ij})^T \int_{\mathrm{Y}_e} \mathbf{B}^T \, \mathbf{E}(\rho_e) \, \mathbf{B} \, \mathrm{d}y \, (\boldsymbol{\chi}^{0(kl)} - \boldsymbol{\chi}^{kl}) =$$
$$\frac{1}{|\mathrm{Y}|} \sum_e (\boldsymbol{\chi}^{0(ij)} - \boldsymbol{\chi}^{ij})^T \, \mathbf{K}_e(\rho_e) \, (\boldsymbol{\chi}^{0(kl)} - \boldsymbol{\chi}^{kl}),$$

where $\mathbf{E}$ is the constitutive matrix, $\mathbf{B}$ is the finite element strain-displacement matrix and $\boldsymbol{\chi}^{0(ij)}$ is the nodal displacement vector corresponding to the test strain field $\boldsymbol{\varepsilon}^{0(ij)}$.

The sensitivity of a component of the constitutive tensor with respect to the density design variable ρ_e can again be found by the adjoint method. The resulting sensitivity expression in FE-notation is

$$\frac{\partial E^H_{ijkl}}{\partial \rho_e} = \frac{1}{|\mathrm{Y}|} (\boldsymbol{\chi}^{0(ij)} - \boldsymbol{\chi}^{ij})^T \, \frac{\partial \mathbf{K}_e(\rho_e)}{\partial \rho_e} \, (\boldsymbol{\chi}^{0(kl)} - \boldsymbol{\chi}^{kl}).$$

Lecture 11: Extensions and Applications – continue - 2

10.2 Objective functions for material design

The goal of material design may be to synthesize a material with prescribed constitutive properties or it may be to synthesize materials with extreme constitutive properties. An example of the former could be the need for designing a material with a specific Young's modulus and a specific isotropic thermal expansion coefficient. This material could be used to neutralize thermal mismatch in a heat generating structure. An example of synthesis of an extremal material could be to maximize the bulk modulus of a material for a given volume fraction of solid material. This would result in a material with an extreme stiffness to weight ratio. For now, we consider the design of materials composed of a solid and a void phase. Therefore, the element stiffness may be interpolated by the SIMP interpolation as we did for structural design problems.

$$E(\rho_e) = \rho_e^p E_0$$

If we want to obtain a material with prescribed elastic tensor E^*_{ijkl}, an objective function to be minimized could be the error between the homogenized elasticity tensor E^H_{ijkl} and the wanted stiffness tensor E^*_{ijkl}. An optimization problem with this goal can be written as

$$\min_{\boldsymbol{\rho}} \sum_{i,j,k,l=1}^{d} (E^*_{ijkl} - E^H_{ijkl}(\boldsymbol{\rho}))^2$$

$$\text{s.t.} : \mathbf{K}\boldsymbol{\chi}^{kl} = \mathbf{f}^{kl}, \quad k,l = 1,\ldots,d\ ,$$

$$\frac{1}{|\mathrm{Y}|}\sum_{e=1}^{N} v_e \rho_e \leq \vartheta,$$

$$0 < \rho_{min} \leq \rho_e \leq 1, \quad e = 1,\ldots,N$$

Lecture 11: Extensions and Applications – continue - 2

where ϑ is the bound on the volume fraction and d is the spatial dimension.

If a material with the wanted properties E^*_{ijkl} cannot be obtained for the given constituent materials and volume fractions, the problem formulation may give useless results. On the other hand, if the wanted properties E^*_{ijkl} are easy to obtain, it means that one could take out material of the base cell and still obtain the wanted properties. This superfluous material tends to cloak the design process and prevent convergence of the optimization algorithm. Also, it paralyses the SIMP scheme since the volume constraint is not active, in turn producing pictures with lots of grey elements.

Alternatively one my turn the problem upside down and minimize the volume fraction for prescribed constitutive properties. This may be formulated as

$$
\begin{aligned}
&\min_{\boldsymbol{\rho}} \ \frac{1}{|\mathrm{Y}|}\sum_{e=1}^{N} v_e \rho_e \\
&\text{s.t.} : \mathbf{K}\boldsymbol{\chi}^{kl} = \mathbf{f}^{kl}, \quad k,l = 1,\ldots,d\ , \\
&\qquad E^*_{ijkl} - E^H_{ijkl}(\boldsymbol{\rho}) = 0, \quad i,j,k,l = 1,\ldots,d\ , \\
&\qquad 0 < \rho_{min} \leq \rho_e \leq 1, \quad e = 1,\ldots,N\ .
\end{aligned}
$$

Lecture 11: Extensions and Applications – continue - 2

For a continuum model of the unit cell, not every positive definite stiffness tensor is realizable, and theoretical bounds on the material parameters for isotropic, square or cubic symmetric composite material are known. This means that the problem formulation may in some cases suffer from lack of any feasible designs. To circumvent this and in order to be able to synthesize extreme materials, i.e. materials with properties that reach the limits of the bounds, we write a new problem formulation as

$$
\begin{aligned}
&\min_{\boldsymbol{\rho}} \; c(E^H_{ijkl}(\boldsymbol{\rho})) \\
&\text{s.t.} : \mathbf{K}\boldsymbol{\chi}^{kl} = \mathbf{f}^{kl}, \quad k,l = 1,\ldots,d \;, \\
&\qquad \frac{1}{|\mathrm{Y}|}\sum_{e=1}^{N} v_e \rho_e \leq \vartheta, \\
&\qquad g_i(E^H_{ijkl}(\boldsymbol{\rho})) \leq g_i^*, \quad i = 1,\ldots,M \;, \\
&\qquad 0 < \rho_{min} \leq \rho_e \leq 1, \quad e = 1,\ldots,N \;,
\end{aligned}
$$

where the objective function $c(E^H_{ijkl})$ and constraints $g_i(E^H_{ijkl})$ are functions of the homogenized tensor and M is the number of constraints.

The problem formulation has been used successfully in the design of material with extremal elastic, thermoelastic, piezoelectric and other physical properties. As will be seen in the following subsections, the results are very close to theoretical limits and have in fact in some cases inspired the improvement of theoretical limits.

Lecture 11: Extensions and Applications – continue - 2

10.3 Material design results

Extremal elastic properties A basic material design problem is to find a structure with maximum bulk modulus for a given volume fraction. This is a highly non-unique optimization problem. Four types of microstructures are now known to have extreme bulk moduli, i.e. they have bulk moduli equal to the upper Hashin-Shtrikman bounds.

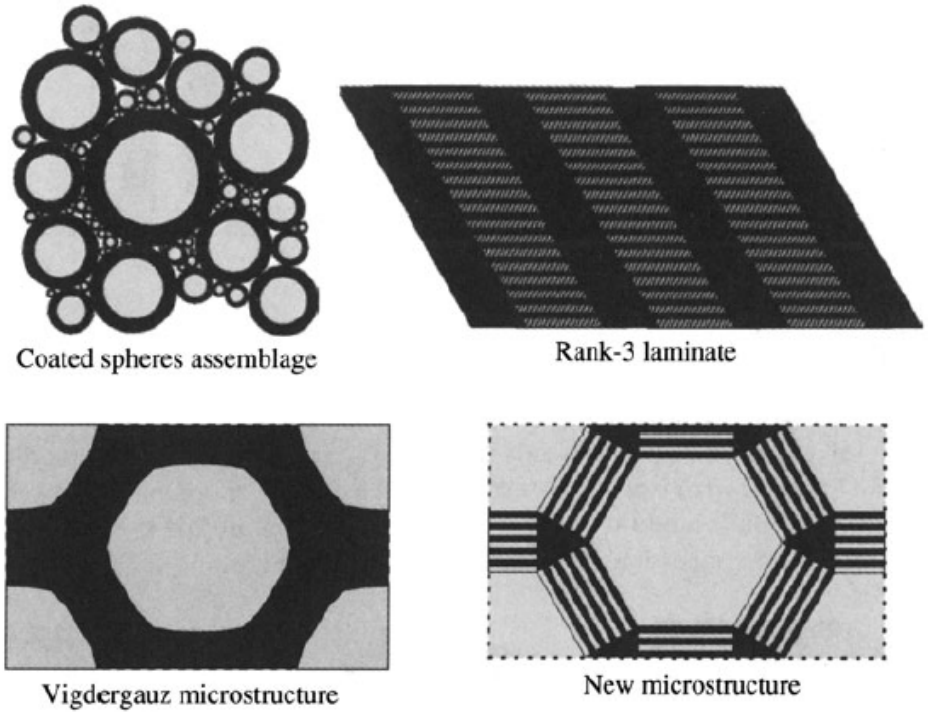

The four known classes of extremal isotropic microstructures. The isotropy requires special geometries of the different unit cells.

Lecture 11: Extensions and Applications – continue - 2

Topology optimization results for the maximization of bulk modulus of two-dimensional microstructures and a one-length-scale constraint are shown below. All four microstructures have effective bulk moduli within a few percent of each other and the known analytical bound. By control of starting guesses, objective functions , base cell geometry and/or isotropy type, one may obtain one structure or another. The results below were obtained for an initial filter radius of 10% of the base cell. The filter size was gradually decreased to zero during the design process. The obtained structures may be denoted one-length-scale microstructures and correspond to the known optimal so-called Vigdergauz structures. Note that the bulk optimized microstructures are closed walled cells.

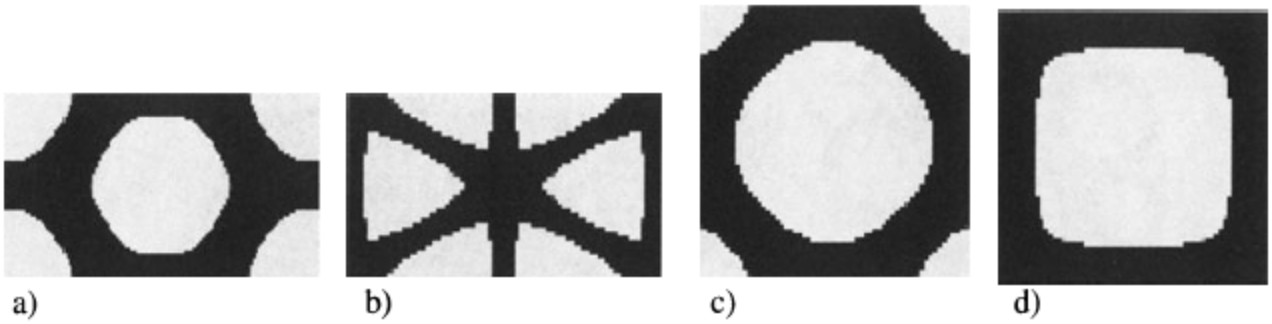

Four microstructures with extremal bulk moduli obtained by the inverse homogenization procedure. a) Isotropic hexagonal microstructure (maximization of bulk modulus for rectangular base cell with isotropy constraint) , b) isotropic triangular microstructure (maximization of product of bulk and shear modulus for rectangular base cell with isotropy constraint), c) isotropic octagonal microstructure (maximization of bulk modulus with isotropy constraint) and d) square symmetric microstructure (maximization of bulk modulus)

Lecture 11: Extensions and Applications – continue - 2

Below shows two examples of maximization of bulk modulus of 3D structures. Again, the two structures that were obtained without and with isotropy constraint have effective bulk moduli extremely close to the theoretical Hashin-Shtrikman bounds.

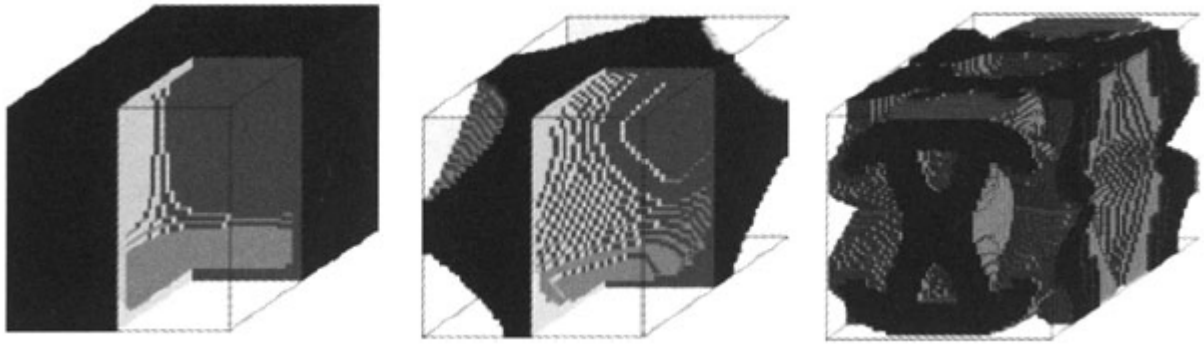

Three optimized three-dimensional microstructures. Left: cubic symmetric maximum bulk modulus microstructure. Center: Isotropic maximum bulk modulus microstructure. Right: Isotopic negative Poisson's ratio material

Lecture 11: Extensions and Applications – continue - 2

A realization of the SIMP model We have continually compared the SIMP and other interpolation models with the Hashin-Shtrikman bounds for isotropic composites. These bounds gives *necessary* conditions for the interpolation models. However, it is the material design methodology of the inverse homogenization method that allows us to construct concrete realizations of the SIMP model, as seen below. Note that, in itself, the inverse homogenization is based on a SIMP interpolation in the unit cell, making the dog bite its tail.

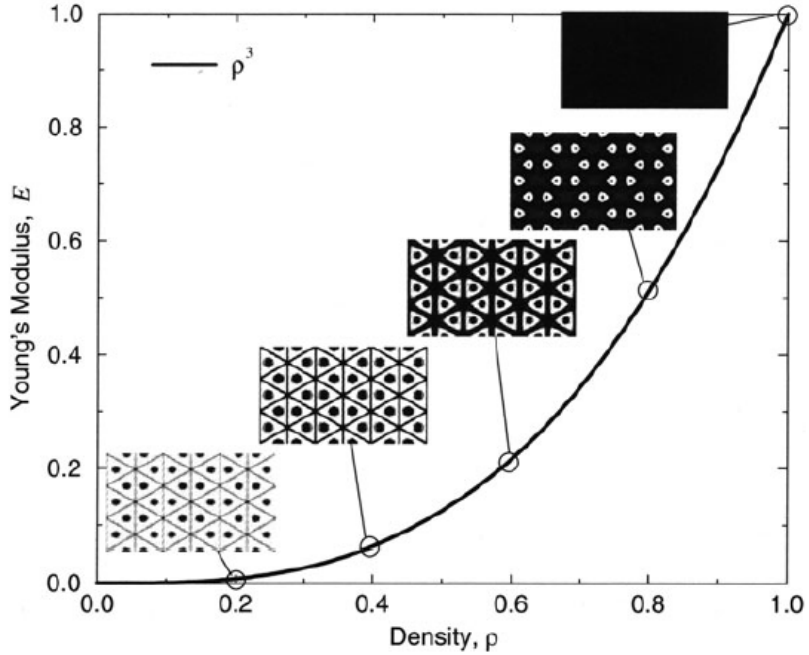

Microstructures of material and void realizing the material properties of the SIMP model with p = 3, for a base material with Poisson's ratio ν = 1/3. As stiffer material microstructures can be constructed from the given densities, non-structural areas are seen at the cell centers

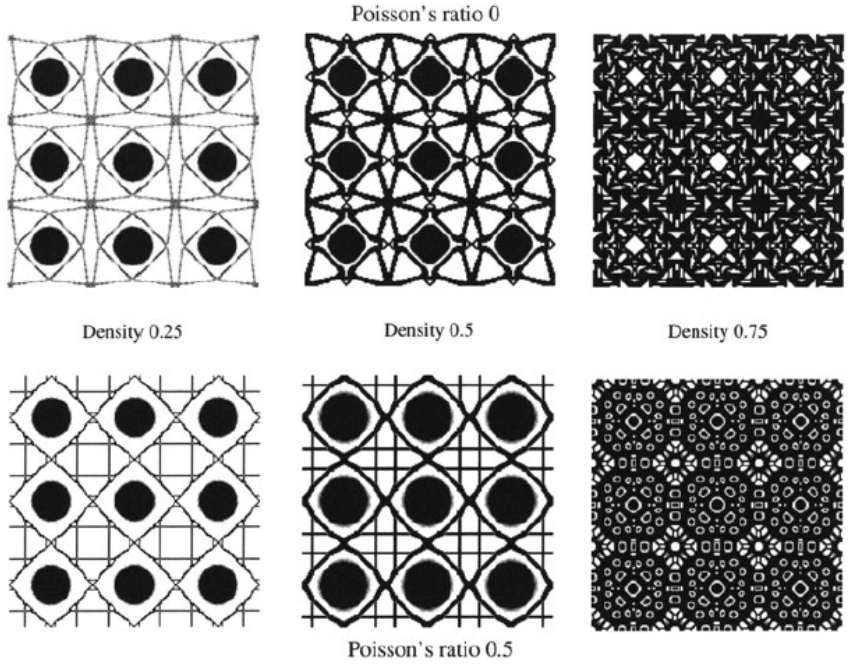

Microstructures of material and void realizing the material properties of the SIMP model with p = 4 for a base material with Poisson's ratio v = 0 (top row) and v = 0.5 (bottom row), respectively. As left figure, non-structural areas are seen at the centers of the cells

Lecture 11: Extensions and Applications – continue - 2

Negative Poisson's ratio materials An extremely interesting application of the material design method is the search for negative Poisson's ratio materials. A number of such structures have been suggested in the literature, but here we apply topology optimization to obtain the behaviour we are looking for. If previous equation is formulated so as to minimize the Poisson's ratio with a constraint on bulk modulus and isotropy, the inverse homogenization method gives results as shown for 2D below.

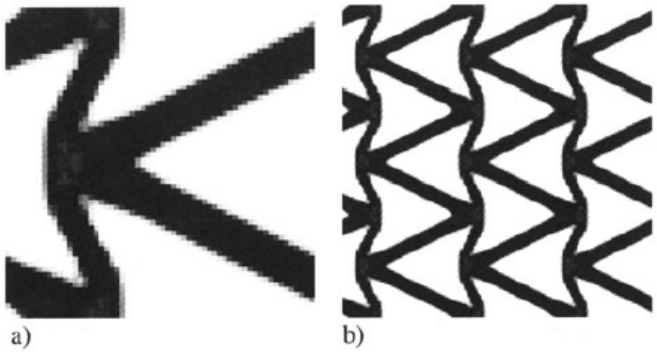

The isotropic and negative Poisson's ratio structure has been manufactured in micro-scale. The 40 by 8 cell test beam was built using surface micromachining with a unit-cell size of 60 *µm* as shown in (c). The Poisson's ratio of the test-beam was measured to -0.9±0.1 in experiments; this compares favourably to the theoretical value of -0.8.

Material microstructure with negative Poisson's ratio. a) one unit cell discretized by 60 by 60 elements, b) repeated unit cell and c) micromachined test beam built at MIC, DTU, DK

Lecture 11: Extensions and Applications – continue - 2

Optimizing the thermal expansion coefficient
For two-phase composites made from solid and void, the effective thermal expansion coefficient will always be the same as for the solid phase, unless the material is disconnected. For two-phase mixtures of two non-void materials, the effective thermal expansion coefficient for any square or cubic symmetric mixture of the materials will always take values between the maximum and the minimum thermal expansion coefficients of the two phases. However, for three-phase composites, it becomes more interesting. According to theory, it is possible to synthesize three-phase materials with effective thermal expansion coefficients that exceed those of the individual phases. In particular, it should be possible to synthesize negative thermal expansion materials from mixtures of two positive expansion phases and a void phase. The extreme thermal expansion is obtained at the cost of a decrease in the effective bulk modulus. The theoretical bounds on the range of attainable combinations of thermal coefficients and bulk modulus for a particular case are shown in (a).

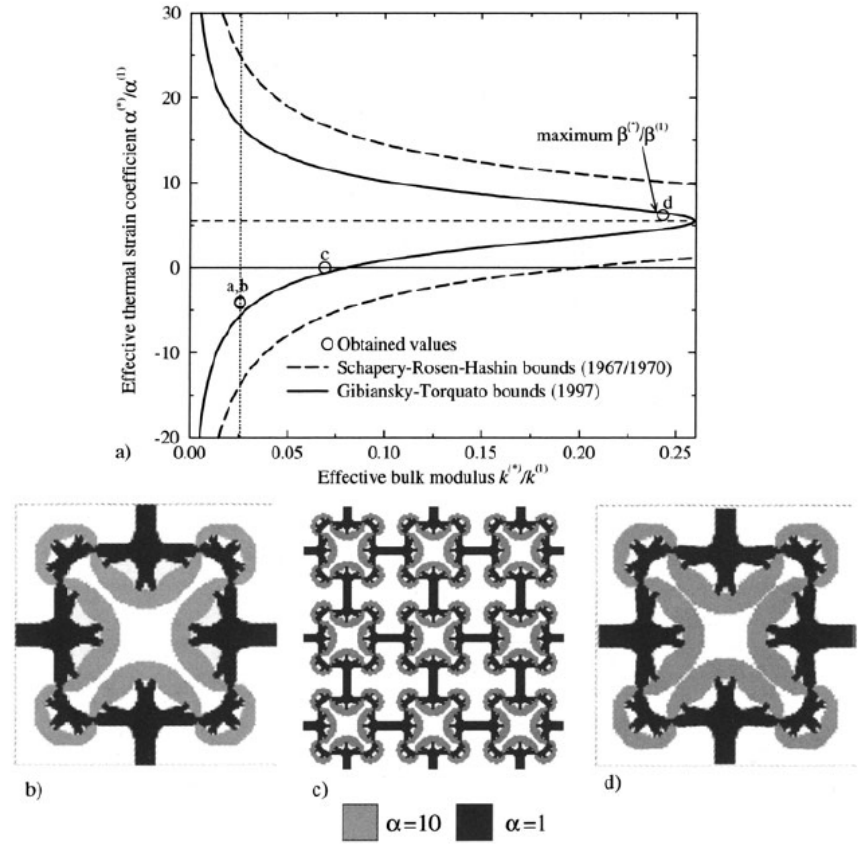

Design of materials with extreme thermoelastic properties using topology optimization. a) Thermal expansion coefficient-bulk modulus graph for specific thermoelastic composite including theoretical bounds and numerically obtained properties, b) , c) and d) material microstructure with negative thermal expansion coefficient (single base cell, 3 by 3 array and heated single cell). When heated, the cell contracts resulting in an effective negative thermal expansion coefficient

Lecture 11: Extensions and Applications – continue - 2

For the design of extremal thermal expansion coefficients it is necessary to extend the previous problem formulation to include an extra load case. This extra load case corresponds to subjecting the base cell to a uniform temperature increase. The new problem formulation may be written as

$$
\begin{aligned}
&\max_{\boldsymbol{\rho}} \; c(E^H_{ijkl}(\boldsymbol{\rho}^1,\boldsymbol{\rho}^2),\; \alpha^H_{ij}(\boldsymbol{\rho}^1,\boldsymbol{\rho}^2)) \\
&\text{s.t.}: \mathbf{K}\boldsymbol{\chi}^{kl} = \mathbf{f}^{kl}, \quad k,l = 1,\ldots,d\;, \\
&\qquad \mathbf{K}\boldsymbol{\chi}^{\alpha} = \mathbf{f}^{\alpha}\;, \\
&\qquad \frac{1}{|\mathrm{Y}|}\sum_e v_e \rho^1_e \rho^2_e \le \vartheta_1, \quad 0 < \rho_{min} \le \rho^1_e \le 1, \quad e = 1,\ldots,N\;, \\
&\qquad \frac{1}{|\mathrm{Y}|}\sum_e v_e \rho^1_e (1-\rho^2_e) \le \vartheta_2, \quad 0 \le \rho^2_e \le 1, \quad e = 1,\ldots,N\;, \\
&\qquad g_i(E^H_{ijkl}(\boldsymbol{\rho}^1,\boldsymbol{\rho}^2)) \le g^*_i, \quad i = 1,\ldots,M\;,
\end{aligned}
$$

where the thermal test field $\boldsymbol{\chi}^{\alpha}$ is again Y-periodic and the thermal finite element load vector is defined as

$$
\mathbf{f}^{\alpha} = \sum_e \int_{Y_e} \mathbf{B}_e^T \mathbf{E}_e(\rho^1_e,\rho^2_e)\; \boldsymbol{\alpha}(\rho^2_e) dY.
$$

Lecture 11: Extensions and Applications – continue - 2

Here, the element thermal expansion coefficient is interpolated by the expression given. The examples shown in the following are all based on the three phase SIMP interpolation scheme. (a) shows a graph of the thermal expansion coefficients as a function of the bulk moduli for some numerically obtained microstructures compared with the theoretical bounds. The design problem consists in extremizing the thermoelastic properties of a composite consisting of 25% of a material with thermal expansion coefficient 10 (normalized value) and 25% of a material with thermal expansion coefficient 1. A resulting composite with a negative thermal expansion coefficient of -4.02 is shown in (b). This shows that it is actually possible to design materials with negative thermal expansion coefficients from constituent phases with positive thermal expansion coefficients. In (a) one notes that the numerically obtained effective values are far away from the old bounds but very close to the newer bounds. In fact, the substantial improvement of the new bounds compared to the old bounds was inspired by the numerical results.

Lecture 11: Extensions and Applications – continue - 2

A new class of extremal two-phase composites Existing bounds on the possible range of the bulk and shear moduli of isotropic two-phase composites composed of isotropic constituents have only been proven optimal (in the sense that there exist microstructures that attain them) for certain cases. In order to investigate the optimality of these bounds in further detail, a study based on the inverse homogenization was performed. The study resulted in numerically obtained bounds for one-length-scale structures, proof of optimality of the bounds in a wider range than previously known and a new class of extremal composites. Thus, use of the topology design methodology has lead to new understanding in the area of theoretical material science. This symbiosis is strongly present when one considers topology design with composites where design has benefited immensely from work in material science.

Limiting the microstructural variation to one length-scale by fixing the value of the mesh-independency filter, one-length-scale bounds on bulk and shear moduli of isotropic two-phase composites shown in (a) below are obtained. These bounds shall not be taken formally but more as bounds based on experience and trust in that the inverse homogenization procedure produces reliable results.

Lecture 11: Extensions and Applications – continue - 2

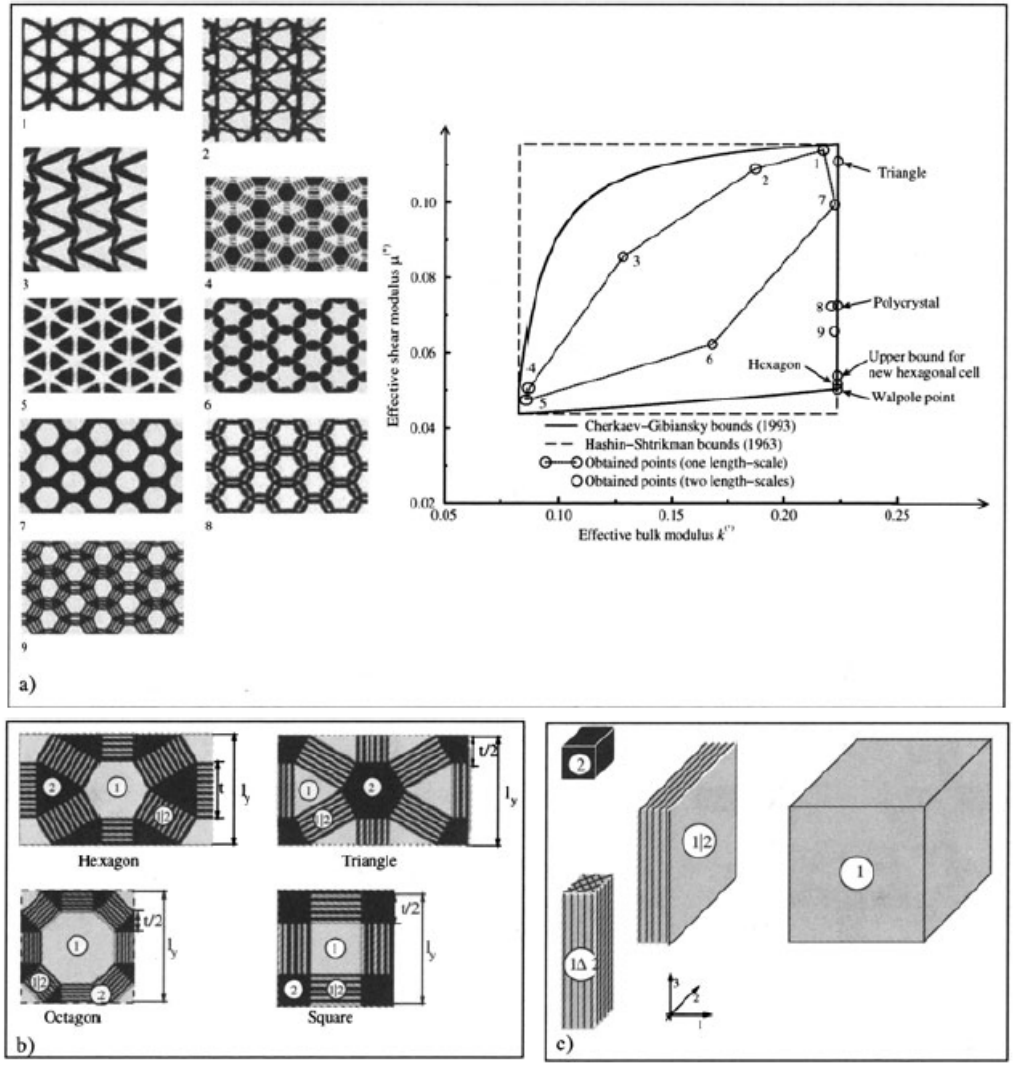

Design of extremal two-phase composites. a) Bound for one-length-scale composites and numerically obtained microstructures and allowing finer variation in the microstructure results in a new microstructure with properties close to the Walpole point (maximum bulk modulus and minimum shear modulus, b) two dimensional members of the new class of extremal microstructures consisting of solid convex polygonal regions connected by laminated bars and c) three-dimensional members of the new class of extremal microstructures

Lecture 11: Extensions and Applications – continue - 2

Studying the bounds based on the one-length-scale structures in (a), one notes that no structures get close to the lower right corner of the bounds, also called the Walpole point (i.e. maximum bulk modulus and minimum shear modulus corresponding to the lower right corner of the bounds). Allowing finer variation in the microstructures by decreasing the filter size, a sequence of designs with properties getting closer and closer to the Walpole point (see a) may be obtained. Inspired by these numerically obtained results, a parametrized hexagonal microstructure consisting of convex polygonal regions of solid material phases connected by layers of equal proportions was investigated analytically (b) . Surprisingly, it was possible to calculate the effective properties exactly and the bulk modulus of the composite corresponded to the Hashin-Shtrikman bounds. Even more surprising, exact solutions and proof of extremity could be obtained for a whole class of similar microstructures in two and three dimensions (see b and c). The investigation thus resulted in a new class of extremal isotropic microstructures which constitutes an alternative to the three previously known classes, namely Composite Spheres assemblages, Vigdergauz structures and rank-N layered materials. One member of this class of materials (the hexagonal microstructure) has maximum bulk modulus and lower shear modulus than any previously known composite. Although no member of the new class of materials attains the Walpole point exactly, the Walpole point can be considered attainable for all practical means and the Hashin-Shtrikman/Cherkaev-Gibiansky bounds have been proven optimal for a wider range of properties than was previously known.

Lecture 11: Extensions and Applications – continue - 2

A new class of extremal three-phase composites Inspired by the two-phase results in the previous subsection the same type study consisting of analytical methods combined with numerical experiments may be performed for three-phase materials. When considering three material phases the equations become much more complicated, and a large number of special cases must be considered for the large number of possible material combinations (e.g. bulk and shear moduli may be well-ordered or not). Nevertheless, the existence of a new class of three-phase composites with extremal bulk moduli can be proved. The three phase microstructures are closely related to the two-phase class from the previous subsection. For example, the three-phase structures converge to the two-phase structures when the volume fraction of one phase approaches zero. For the three-phase case, the new class of structures also expands the ranges of previously known attainable properties and optimality of bounds. (a) shows some numerically obtained three-phase microstructures and (b) shows schematics of members of the new class of three-phase extremal microstructures. Note how *layered* regions again play a significant role.

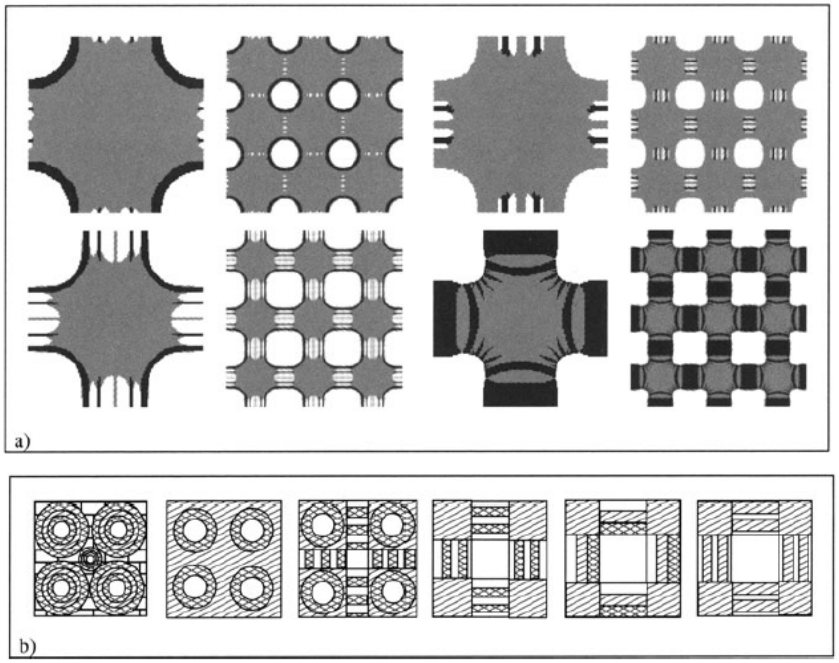

Design of extremal three-phase composites. a) Numerically obtained three-phase microstructures with extremal bulk modulus, b) schematics of the new class of extremal microstructures

Lecture 11: Extensions and Applications – continue - 2

Piezoelectric sensors Another three-phase material design example is the design of hydrophones based on piezoelectric sensing. A piezoelectric material responds with an electric output when strained. For a typical ceramic piezoelectric rod, the electric field depends on the elongation of the rod. Simply said, this means that the electric output for a horizontal compression will have the negative sign of a that for a longitudinal compression. For hydrophones which should detect changes in hydrostatic pressures, this is a problem. Compression in all directions simultaneously will almost cancel the electrical output. In order to circumvent this problem it has been suggested to embed piezoelectric rods in a matrix material with tailored properties. A negative Poisson's ratio matrix material will for example convert transverse pressure to a compression of the rod instead of extension, in turn causing a much larger output signal. The inverse homogenization method may be used to identify the matrix microstructure that maximizes the electric output of hydrophones.

The problem corresponds to a three-phase material design problem of distributing a piezoelectric, a polymer and a void phase in a periodic base cell. However, for various reasons, the periodicity of the matrix microstructure will often be much smaller than for the embedded rods. Therefore one may model the problem partly by effective medium theory and partly by numerical homogenization. This means that the effective properties of the matrix material may be found by numerical homogenization whereas the effective properties of the mixture of the matrix material and the piezoelectric rods may be found analytically. The effective piezoelectric properties may thus be determined directly as functions of the effective matrix properties E_{ijkl}. The optimization problem may then be solved by the extremal material design formulation. (b) shows one base cell of the matrix material of a hydrophone optimized for maximum piezoelectric charge coefficient. One observes that this matrix material is a transversely isotropic material with negative Poisson's ratio. The improvement compared to a solid polymer matrix is a factor of 11. (c) shows a base cell (5 mm cubed) manufactured using stereolithography.

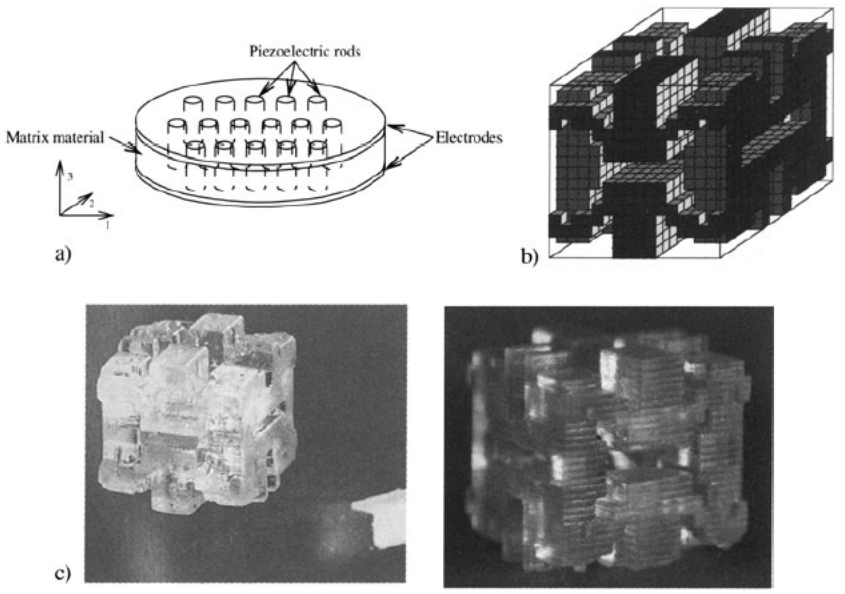

Design of hydrophones using topology optimization. a) Schematic of a 1-3 piezoelectric hydrophone, b) one base cell of hydrophone matrix optimized for piezoelectric charge coefficient and c) one base cell manufactured using stereo-lithography

Thank you for your attention